An Infrared Photon-counting Photometer
Based on the Edge-illuminated Solid-State Photomultiplier

Dae-Sik Moon[1234], Stephen S. Eikenberry[54], and Giovanni G. Fazio[6]

[1]Division of Physics, Mathematics and Astronomy, Caltech, MC 103–33, Pasadena, CA 91125;
[2]Robert A. Millikan Fellow;
[3]Space Radiation Laboratory, Caltech, MC 220–47, Pasadena, CA 91125;
[4]Department of Astronomy, Cornell University, Ithaca, NY 14853;
[5]Department of Astronomy, University of Florida, Gainesville, FL 32611;
[6]Harvard-Smithsonian Center for Astrophysics, 60 Garden Street, Cambridge, MA

ABSTRACT

We present the design, construction, and test observations of a new infrared (IR) photon-counting photometer for astronomy based on the edge-illuminated solid-state photomultiplier (EISSPM). The EISSPM has a photon-counting capability over the 0.4–28 μm range with a nanosecond-scale intrinsic detector time resolution. Its quantum efficiency (QE) peaks ≥ 30 % in the near-IR, which is much higher than the previous SSPM with back illumination. After characterizing the dark noise of the EISSPM at its operational temperature range, we develop an EISSPM-based IR photon-counting photometer for astronomical observations. This includes the design and construction of a full optical, cryo-mechanical, and electronics system as well as the software for operating the instrument on telescopes. We report the results of our test observations of the Crab Nebula pulsar using this new instrument on the Palomar Hale 5-m telescope with 10-μs time resolution.

Keywords: infrared, instrumentation, detectors, photometers

1. INTRODUCTION

A photon-counting capability with > 100 Hz sampling rate (and potentially up to $\sim 10^6$ Hz sampling rate) has diverse interesting applications in modern astronomy, involving both observational and technological aspects. This includes studies of the rapid periodic/aperiodic variabilities from compact sources (such as pulsars and X-ray binaries), the planetary and lunar occultations, the fringe detection in the IR interferometry, and the wavefront sensing in the adaptive optics. (Note that the latter two are exclusively for the IR wavebands.) In the X-ray waveband, the fast timing analysis is already a vital component for studying compact objects as manifested by the recent success of the Rossi X-ray Timing Explorer. However, in the IR waveband, it was only a few years ago when the first (and still unique) prototype high-speed IR photon-counting photometer, which was based on the back-illuminated SSPM (BISSPM), was introduced.[1]

Although the advent of the BISSPM-based photometer led the detailed multi-wavelength (from the γ-ray to near-IR waveband) study of the pulsations of the Crab Nebula pulsar[2] owing to its superb time resolution, many other aspects of the instrument have remained to be improved. *First*, the detector QE is very low (a few percents), limiting its applications only to bright objects. *Next*, the instrument lacks the capability of changing the apertures and filters over a given night. *Finally*, the readout system relies on the out-of-date electronics, making it difficult to carry out efficient astronomical observations.

Here, we report the design, construction, and performance of a new IR photon-counting photometer based on the EISSPM.* The EISSPM has a much higher QE (≥ 30 % in the near-IR waveband) than the BISSPM, and the new photometer is capable of changing the apertures and filters at any given time. In addition, we have already developed new readout electronics optimized for IR/optical photon-counting photometers.[3] Thus we now have a complete and efficient system for high-speed, photon-counting astronomical observations in the near-IR waveband. We describe the EISSPM photometer below.

Send correspondence to D.-S.M.: moon@srl.caltech.edu
*The both BISSPM and EISSPM detectors have been developed by Rockwell Scientific.
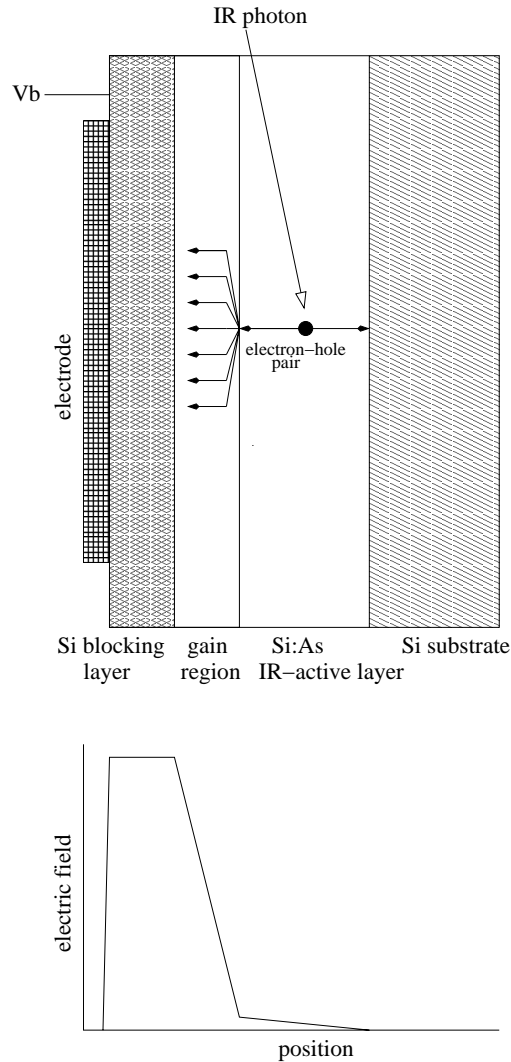
Figure 1. A simplified cross-section of the EISSPM. Note that it is not to the exact scale.

2. THE DETECTOR AND OPTICAL SYSTEM

2.1. The detector: EISSPM

The EISSPM is basically an arsenic-doped-silicon (Si:As) blocked-impurity band (BIB) detector. Its spectral coverage is 0.4–28 μm, similar to that of a conventional Si:As BIB detector. A major difference of the EISSPM from a normal Si:As BIB detector is the existence of a gain region, which is implemented by Boron counter-doping, between an IR-active layer (i.e., Si:As) and a blocking layer of intrinsic silicon. It is this gain region which makes the EISSPM an avalanche-mode Si:As BIB detector capable of photon counting. As shown in Figure 1, at the proper temperature of ∼5–8 K, a bias V_b (typically $\simeq -11$ V) develops a strong electric field in the gain region where a photo-electron produced by an incident IR photon in the Si:As layer generates an avalanche of ∼40,000 electrons with an intrinsic pulse width of a few nanoseconds.

Figure 2 shows a block diagram of the EISSPM detector package that we have used. The package contains the EISSPM, a temperature-sensing diode, a 150-Ω heater, and two holes for the standard 4-40 screws. The size of the EISSPM is 100×45 μm^2 and its path length is 1 mm, while the 100 μm width extends to 300 μm along the path. For comparison, the size of the BISSPM is 200×200 μm^2, with 23 μm path length. Because the
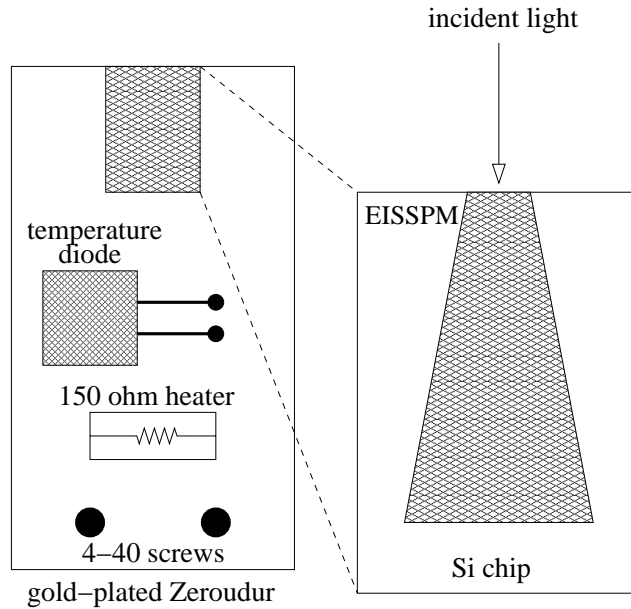
Figure 2. A block diagram of the EISSPM detector package from Rockwell Scientific. Note that it is not to the exact scale.

path lengths of the incident photons in the EISSPM are larger than those of the BISSPM, the QE of the former (≥ 30 %) is much higher than that of the latter (a few %). The larger volume of the EISSPM, however, produces larger thermal dark noise than the BISSPM.

As in Figure 2, the 150-Ω heater is directly exposed to the detector, which can be a significant noise source. In order to avoid this potential noise, we built an oxygen-free copper plate to have the same size of the detector package, and placed it beneath the detector package, with a new 100-Ω hidden resister in the plate just below the EISSPM. We then measured the dark counts of the EISSPM as a function of the bias voltage and temperature inside a liquid Helium dewar using the new heater. Figure 3, which presents the distributions of the dark counts measured with 50 mV discriminating level, shows that the dark counts suddenly increase at $T \geq 7.5$ K while it gradually decrease when the EISSPM is more weakly biased.

2.2. Optical System

Figure 4 presents the full optical system of the EISSPM photometer, consisting of four lenses (two ZnSe lenses for reimaging and the other two CaF$_2$ lenses for converting the telescope f-ratio), an one-inch diameter plane-parallel ZnSe dewar optical entrance window, an aperture wheel with five aperture holes for 2–6 arcsecond field of views, a filter wheel with JHK_s filters, and a Lyot stop. The reimaging part with the two ZnSe lenses is optimized for an f/16 beam (i.e., the Cassegrain f/16 secondary of the Palomar Hale 5-m telescope), while the two CaF$_2$ lenses just in front of the dewar entrance window are designed to efficiently convert an incoming f/8 beam to f/16 when the EISSPM photometer is used on the telescopes with f/8 secondaries (such as the Keck, MMT, and CTIO 4-m telescopes). All the lenses, together with the dewar optical entrance window, were fabricated at Janos Technology and were anti-reflection coated in the 1–5 μm range. The one-inch diameter JHK_s filters were fabricated at Barr Associate for the recent consortium for IR astronomical filters.[4, 5]

The special fan-out structure of the EISSPM (Figure 2) requires an incoming beam (after the reimaging) of f/3 (or slower) to have higher QEs (i.e., longer path lengths), which is difficult to achieve because the field of view of an f/3 (or slower) beam on the EISSPM is smaller than one arcsecond when it is used on relatively large telescopes (e.g., the Palomar 5-m Hale telescope). In order to avoid this contradiction, we positioned the detector slightly (i.e., $\sim$1 mm) behind the focus of the second ZnSe lens (Figure 4), allowing a three-arcsecond field of view with an f/2.5 incident beam. We then evaluated the efficiency of this approach by simulating one thousand
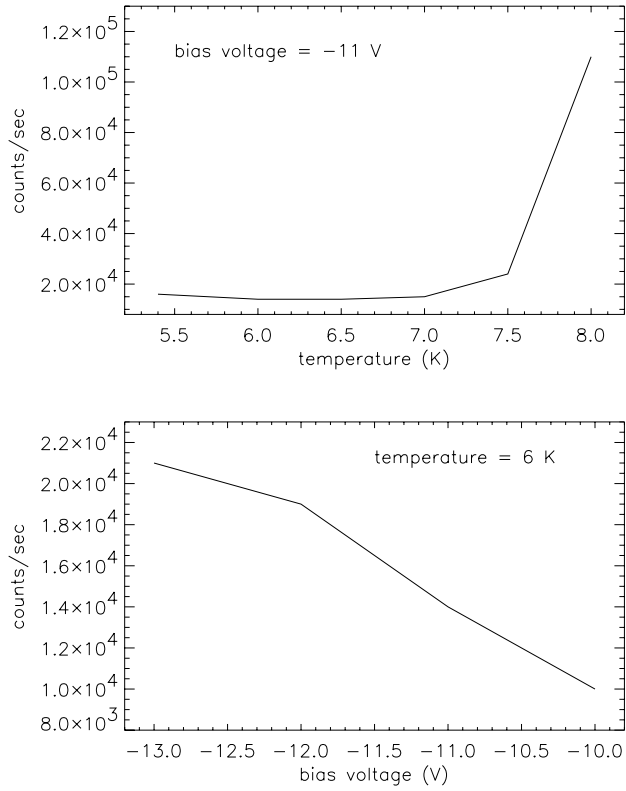
Figure 3. The distributions of the EISSPM dark counts as a function of the bias voltage and temperature. The discrimination level was set to be 50 mV.
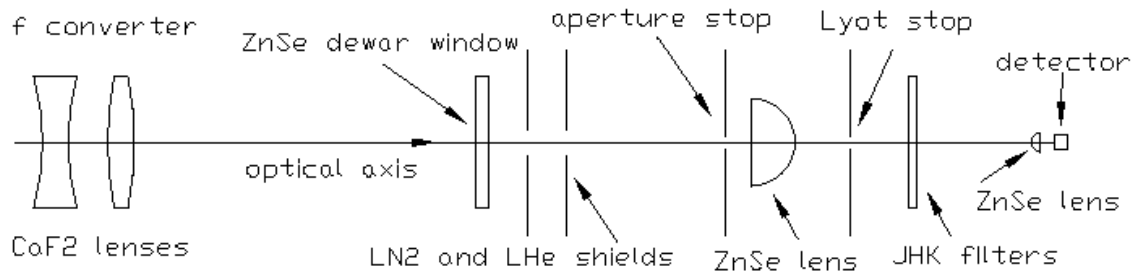
Figure 4. The optical components of the EISSPM detector. Note that the two f-converting CaF$_2$ lenses are outside the dewar.
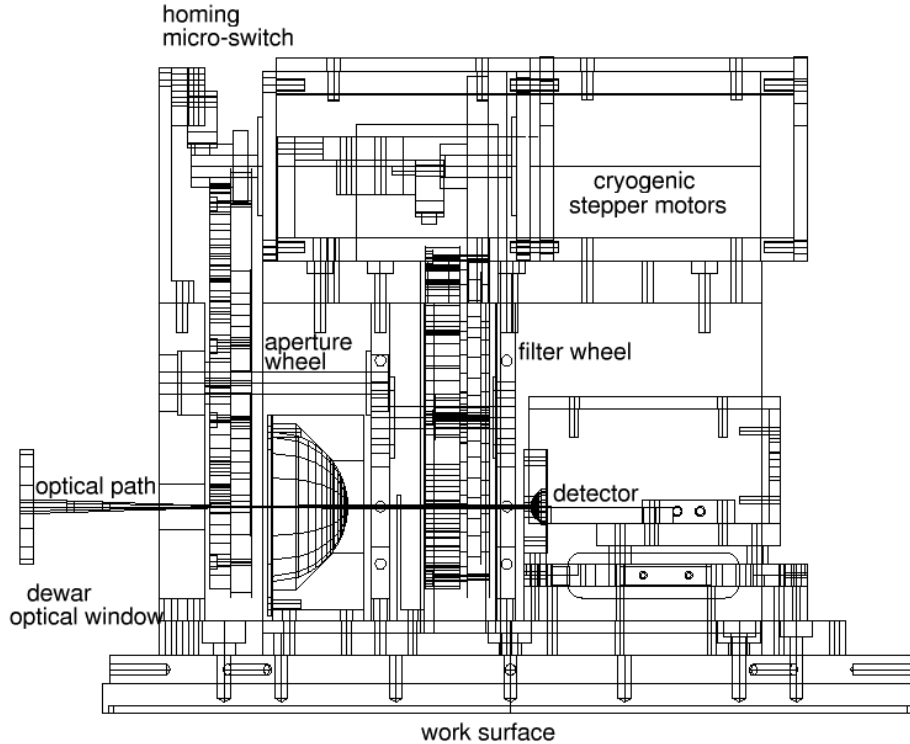
Figure 5. A projected side view of the dewar work surface of the EISSPM photometer, including the optical path of incoming f/16 beam through the entrance window and reimaging lenses, aperture and filter wheels, two stepper motors and their homing micro-switches, lens holders, and detector mount.

artificial photons in a three-arcsecond field of view and tracing them through the full optical system to the detector. In the simulations, the distribution of the thousand artificial photons was convolved with a Gaussian profile of one-arcsecond width to take into account of a typical seeing, and we also assumed the existence of 10 % random variation of the detector QE and one-arcsecond accuracy of the telescope tracking. As a result, we found that ~70 % overall efficiency of this approach compared to the ideal case in which all the photons are incident to the detector perpendicularly. The variations of the calculated overall efficiencies caused by the non-uniform detector QE and the telescope movement were estimated to be ~6 %.

3. MECHANICAL PARTS AND CRYOSTAT

For the EISSPM photometer, we built a dewar having two three-liter cryogenic cans for containing liquid Nitrogen (the outer can) and liquid Helium (the inner can). The size of the dewar copper work surface is 7 inches, while the outer diameter of the dewar is 8.5 inches. Just above the dewar, we placed a base plate made of Invar which holds all other components. Most of the cryostat (such as lens holders and detector mount) are also made of Invar, while we used commercially available Aluminum gears for the filter and aperture wheels. The detector mounting system was designed to be capable of three-dimensional adjustment for the optical alignment. We used two cryogenic stepper motors from Phytron for controlling the filter and aperture wheel at the liquid Helium temperature. Figures 5 presents a projected view of the dewar work surface with all the mechanical parts and cryostat assembled, as well as the two ZnSe lenses and the traces of an incoming f/16 beam.
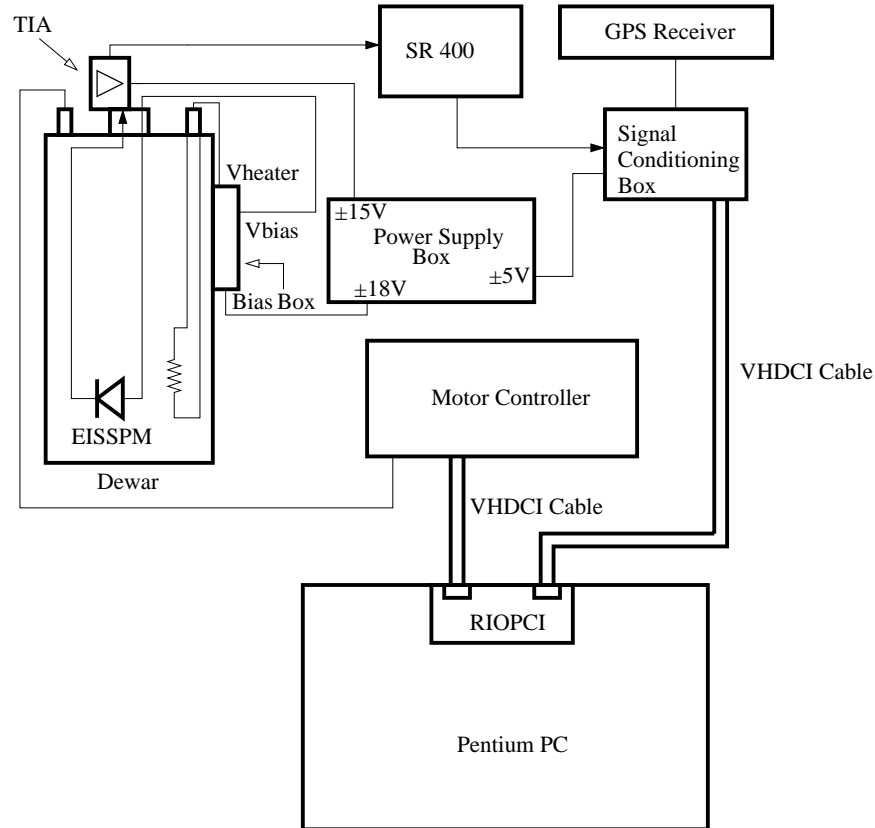
Figure 6. A block diagram of the electronics setup for the EISSPM photometer

4. ELECTRONICS AND SOFTWARE

The electronics and software of the EISSPM photometer are capable of [1] providing a stable bias to the detector and also a power to the heater, [2] converting the detector output current to voltage with sufficient amplification, [3] counting photons at 1 MHz bandwidth and with 1 μs accuracy, and [4] controlling the filter and aperture wheels. For [1] and [2], we implemented a simple circuit mainly based on operational amplifiers, and used a transimpedance amplifier from Rockwell Scientific. All the components for [1] and [2] were directly attached to the dewar. For [3] and [4], we improved our CHISDAS[3] data acquisition system, which was initially developed for high-speed IR/optical photon-counting photometers. Although CHISDAS was originally incapable of [4] (while it was capable of [3]), we have implemented [4] by developing a new Field Programmable Gate Array (FPGA) program and configuring an Altera FPGA chip on the RIOPCI card (see Figure 6) of CHISDAS. Note that CHISDAS is an FPGA-based data acquisition system. We also built a motor controller box which houses two SINCOS stepper drivers from Phytron to control the aperture and filter wheels.

Figure 6 shows a block diagram of the electronics of the EISSPM photometer. The typical operation can be summarized as follows: at the proper bias and temperature controlled by Bias Box, the detector generates pulses of electrons to the TIA where the input current is converted to the output voltage. The output voltage from the TIA then discriminated by Stanford System SR400 Photon Counter at the typical discrimination level of 30–50 mV. After that, the Signal Conditioning Box converts signals from SR400 to digital signals and sends them to the RIOPCI card in the computer through one VHDCI cable, together with timing information from the GPS receiver. The other VHDCI cable from the RIOPCI card is connected to Motor Controller to control the filter and aperture wheels.
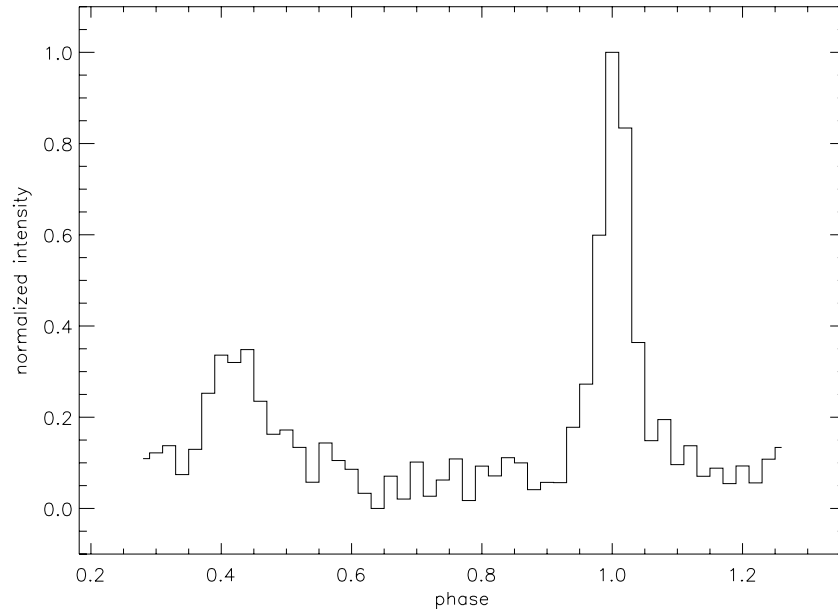
Figure 7. K_s-band Crab Nebular pulsar pulse profile obtained with the EISSPM photometer in 2004 October. The integration time was 10 minutes under a poor weather condition.

5. TEST OBSERVATIONS

Before we carried out real observations, we first tested the performance of the EISSPM photometer. In the laboratory, at the $\sim$6.8 K detector temperature and –9.0 V bias voltage, the photon counts reached $\sim$17000 with the dewar entrance window blocked, while they increased to $\sim$22000 when the dewar entrance window was open. We then illuminated the optical entrance window with normal flash lights to increase the photon counts up to $\sim$53000. Over these measurements, the aperture was fixed to the largest one on the aperture wheel, while the filter wheel was fixed to an open position. Also the SR400 discrimination level was set to be 50 mV. After we rotated the aperture wheel to block the incident light, the EISSPM photometer was insensitive to the flash light illumination, indicating that the instrument was working properly.

In 2004 October 30, we used the EISSPM photometer on the Palomar Hale 5-m telescope for test observations of the Crab Nebula pulsar with 10-μs time resolution. Over the observations, the sky condition was very poor, with variable seeing of $\geq$5 arcseconds and also with occasional heavy clouds. Figure 7 presents a resulting K_s-band pulse profile of the Crab Nebula pulsar integrated over 10 minute exposure with the EISSPM photometer.

REFERENCES

1. S. S. Eikenberry, G. G. Fazio, and S. M. Ransom, "An SSPM-Based High-Speed Near-Infrared Photometer for Astronomy," *PASP*, **108**, pp. 939–943, 1996
2. S. S. Eikenberry, G. G. Fazio, S. M. Ransom, J. Middleditch, J. Kristian, and C. R. Pennypacker, "High Time Resolution Infrared Observations of the Crab Nebula Pulsar and the Pulsar Emission Mechanisms," *Astrophysical J.* **477**, pp. 465–474, 1997

3. D.-S. Moon, B. E. Pirger, and S. S. Eikenberry, "A Next-Generation High-Speed Data Acquisition System for Multichannel Infrared and Optical Photometry," *PASP*, **113**, pp. 646–651, 2001

4. A. T. Tokunaga, D. A. Simons, and W. D. Vacca, "The Mauna Kea Observatories Near-Infrared Filter Set. II. Specifications for a New JHKL'M' Filter Set for Infrared Astronomy," *PASP*, **114**, pp. 180–186, 2002

5. D. A. Simons, and A. T. Tokunaga, "The Mauna Kea Observatories Near-Infrared Filter Set. I. Defining Optimal 1?5 Micron Bandpasses," *PASP*, **114**, pp. 169–179, 2002